IEEE Access
Multidisciplinary ⋮ Rapid Review ⋮ Open Access Journal

Received December 21, 2020, accepted January 8, 2021, date of publication January 18, 2021, date of current version January 27, 2021.

Digital Object Identifier 10.1109/ACCESS.2021.3052567

Deep Convolutional Neural Network for Passive RFID Tag Localization Via Joint RSSI and PDOA Fingerprint Features

CHAO PENG, HONG JIANG, (Member, IEEE), AND LIANGDONG QU
College of Communication Engineering, Jilin University, Changchun 130012, China

Corresponding author: Hong Jiang (jiangh@jlu.edu.cn)

This work was supported in part by the National Natural Science Foundation of China under Grant 61371158 and Grant 61771217, and in part by the Jilin Provincial Natural Science Foundation of China under Grant 20180101329JC.

ABSTRACT Radio-frequency identification (RFID) localization has drawn much attention with the emergence of the Internet of Things (IoT). Deep learning with applications to RFID localization owns a lot of advantages. In this paper, we present a deep convolutional neural network (CNN)-based approach for passive RFID tag localization exploiting joint fingerprint features of the received signal strength indication (RSSI) and phase difference of arrival (PDOA). First, the RSSI and PDOA data are extracted from the received signals of RFID readers. Then, a CNN with three convolution layers and pooling layers is design, in which the normalized RSSI and PDOA data are formed into images as its input to train the weights in the offline stage. In the online stage, the RSSI and PDOA data of test tags are collect and then the positions of unknown tags is predected based on the designed CNN. In the simulations, the accuracy of the proposed approach is compared with several fingerprinting-based schemes such as LANDMARC, weighted K-nearest neighbor (WKNN) and deep neural network (DNN), and the impact of different fingerprint data sets and noise variances on the positioning accuracy is analyzed. Experiments show that the proposed approach can locate multiple tags with high accuracy and stability in complex indoor environment, and outperforms other existing schemes.

INDEX TERMS Radio-frequency identification, indoor localization, convolutional neural network, fingerprint feature, phase difference of arrival.

I. INTRODUCTION

In recent years, indoor localization via radio-frequency identification (RFID) technology [1]–[6] has drawn much attention with the emergence of the Internet of Things (IoT). RFID is a kind of non-contact automatic data acquisition technology using space electromagnetic wave as transmission medium. It has many advantages such as small size, mature technology, high speed, low power consumption, large capacity, anti-interference, long life and high precision [7], [8]. RFID localization has great potential for a variety of IoT applications such as logistics management [9], intelligent purchase guidance [10], medical services [11] and public safety [12], etc. Among them, the implementation of high accuracy positioning of IoT devices with large-scale deployment is crucial [13]. Unlike outdoor localization, which is handled with global positioning system (GPS) and exploits the line-of-sight (LOS) transmission paths, indoor localization faces huge challenges of complex propagating scenarios [14]–[19] such as shadowing effect, multipath propagation, delay distortion, non-line-of-sight (NLOS), and fading [20]–[22], which deteriorate the positioning performance.

Traditionally, range-based methods such as time of arrival (TOA), time difference of arrival (TDOA) [23], angle of arrival (AOA) [24] and received signal strength indication (RSSI) are mainly used in RFID localization. However, their accuracies cannot meet the requirement in actual environment. Recently, the fingerprinting-based approach has become a promising technology for indoor localization, in which the fingerprint database with thorough measurements of the scene is established, then the new measurements are collected and compared with the data in database to achieve positioning. By using the RSSI as measurements, some fingerprinting-based RFID localization approaches have been put forward [20], [25]–[28]. Typically, in [26], LANDMARC system was proposed for RFID localization based on RSSI, which was realized by placing readers and

The associate editor coordinating the review of this manuscript and approving it for publication was Kai Yang.

multiple reference tags. In [20], the weighted K-nearest neighbor (WKNN) approach was presented to improve the location accuracy of KNN [29]. Besides RSSI, several phase-based RFID localization methods have also been investigated [30]–[38].

Despite the fact that these methods can make better use of the survey data than the traditional range-based techniques, they have much limitation on fully exploiting the data and localizing the massively deployed RFID tags on IoT devices. For example, there inevitably exists noise in the datasets, which cannot be well processed with these traditional fingerprinting-based algorithms due to the inability to conduct deep learning on the data. Thus the positioning accuracy cannot be further improved. In this paper, we address to deep learning with applications to RFID indoor localization. To simplify the positioning model, we neglect the problem of signal multiplexing and resource scheduling brought by massive RFID tags.

More recently, deep learning [39] has become an emerging technology in large data analysis and learning. Typically, it contains deep neural networks (DNN) [40], deep belief network (DBN) [41] and convolutional neural network (CNN) [42], etc. In [42]–[44], deep learning for WiFi-based indoor localization has been investigated to obtain high accuracy. In [45], deep learning approach for fingerprinting-based RFID indoor localization has been proposed in our previous work. Different from conventional fingerprint location methods, deep learning-based schemes for RFID indoor localization have a lot of advantages which are itemized as follows. It consists of two stages: offline training and online testing.

1) In the offline training stage, the reference RFID tags are arranged in the localization scene, and the fingerprint database is established by collecting the survey data from the reference tags. The fingerprint data features and training parameters are deeply learned by building a neural network model, thus CNN can learn data in depth and adapt well to the complex indoor electromagnetic interference environment.

2) In the online testing stage, the test data are used as the input of neural network for position estimation, and the probability is the output at each reference point using neural network model, thus the estimated location is calculated as a weighted average of the candidate locations.

In this paper, the deep CNN is applied to RFID multi-tag localization with joint fingerprint features of the RSSI and the phase difference of arrival (PDOA). The CNN for RFID localization has great advantages such as the capability of processing a large amount of data, extracting and training fingerprint features, sharing the parameter structure, and reducing the complexity of neural network. Therefore, the accuracy and real-time of positioning can be guaranteed. In our simulation work, the CNN is designed with three convolutional layers, three pooling layers and one fully connected layer. The convolutional layer and pooling layer can extract image feature information, reduce feature dimension and share parameters.

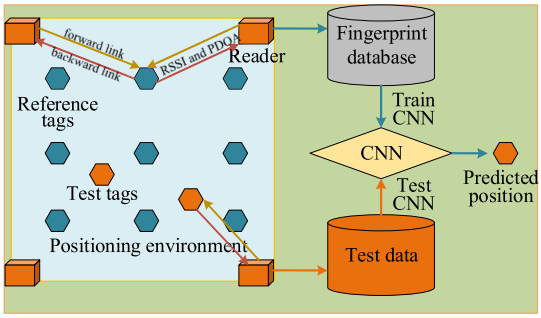

FIGURE 1. Outline of the RFID tag localization system.

To prevent gradient dispersion, ReLU is used as the activation function in our CNN model. Then, the full connection layer is exploited as a classifier to calculate the probability distribution by Softmax function. The outline of the RFID tag localization system is shown in Fig. 1.

In our work, we extract the joint fingerprint features including the RSSI and PDOA from the RFID reader and reference tags in the offline stage. Considering the propagation scene of RFID signals with path-loss and phase-distance models, we collect the joint RSSI/PDOA measurements of the reference tags and normalize them. The fingerprint data are made into images with size 32×32 as the input of the CNN to train its weights by deeply learning the features of images. For comparison, three kinds of training datasets are generated including RSSI, PDOA and joint RSSI/PDOA, respectively, and a back propagation algorithm (BP) [43] is used to train their weights. In the online stage, the same three kinds of test datasets are collected and the trained CNN model is used to estimate the position of the test tags. Finally, the effects of the three different fingerprint datasets as well as the varying noise variances on positioning accuracy are analyzed. Experimental results show that the CNN-based approach outperforms several existing localization schemes, which has higher accuracy and stability.

The main contributions of this paper are as follows:

1) We extract the joint fingerprint features including RSSI and PDOA measurements for RFID positioning, and experimentally validate the effectiveness of RFID localization using joint RSSI/PDOA datasets.
2) We design a deep CNN with three convolution layers and three pooling layers to train the RFID fingerprint data in the offline stage.
3) We use the probability distribution of the test tag at each reference point, rather than its coordinate, as the output of the CNN, and select the K positions with the highest probability to improve the RFID positioning accuracy.

The remaining of this paper is organized as follows. Section II introduces the data collection of RSSI and PDOA. Section III investigates the CNN-based RFID tag localization approach via joint fingerprint features. Section IV gives the analysis of experimental results and Section V concludes this paper.

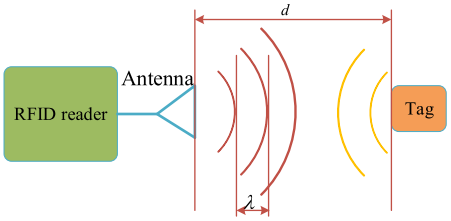

FIGURE 2. Forward link and backward link propagation mode of RFID.

II. DATA COLLECTION OF RSSI AND PDOA

A. RSSI AND PDOA MEASUEREMENT MODEL

The illustration of RFID forward and backward link propagation is shown in Fig. 2. RFID reader establishes communication with tag through the half duplex communication mode of reader first speech [46]–[48]. Therefore, RFID communication includes two links, forward link and backward link. In RFID communication system, the reader antenna transmits interrogation signals towards surrounding passive tags. After receiving the transmitted signal, the tag activates itself with the signal energy, and then backscatters the signal to the reader antenna [3]. The RSSI and PDOA values can be extracted from these signals by measurements.

In practice, complex environment will affect the transmission of wireless signal. We exploit the logarithmic path-loss model to simulate the propagation of RFID signals. According to [25], RSSI can be mathematically determined by

$$RSSI[dBm] = P_t[dBm] + G_t[dBi] + G_r[dBi] - P_L(f, d)[dB] + X_\sigma \quad (1)$$

where

$$P_L(f, d) = 10n\log_{10}\left(\frac{4\pi f}{c}\right) + 10n\log_{10}(2d) \quad (2)$$

In (1), P_t denotes the power of the transmission signal from the RFID reader. G_t and G_r are the gains of the RFID reader transmitter and receiver antennas, $P_L(f, d)$ in (2) denotes the path loss when the carrier frequency is f and the distance between the RFID reader and tag is d, whose unit is dB. c is the speed of light. n is the path loss constant, which denotes the rate of path loss increasing with distance, and it depends on the surrounding environment and the material type of the building. $X_\sigma \sim \mathcal{N}(0, \sigma_1^2)$ represents Gaussian distributed noise with zero mean and variance σ_1^2.

The PDOA, i.e., the phase difference of arrival ϕ, is generated during the forward and backward propagation. Not only the spatial distance between the RFID reader and the tag but also the hardware circuits, multipath and transmission line effects may introduce phase rotation. In practice, the measured phase cannot be directly used in RFID systems since it is wrapped into multiple of 2π. The phase unwrapping method has been studied in [30], here we assume that the phase information has been well unwrapped. Thus, we can express the basic phase-distance model as

$$\begin{cases} \phi = \phi_p + \phi_e \\ \phi_p = \dfrac{4\pi d}{\lambda} \\ \phi_e = \dfrac{4\pi d Z_\sigma}{360} \end{cases} \quad (3)$$

where $\lambda = c/f$ denotes the wavelength of the RF signal. ϕ denotes the observation value of phase difference reported by the RFID reader, ϕ_p denotes the phase rotation due to the propagation delay, and ϕ_e is the phase error caused by hardware circuits, multipath, and transmission line effects. In this paper, we assume that the phase disturbance Z_σ (regarded as noise) obeys Gaussian distribution $\mathcal{N}(0, \sigma_2^2)$, with mean μ and variance σ_2^2. In Fig. 2 the total spatial propagation distance of the RF signal is $2d$ due to the forward and backward propagations during the backscatter communication.

B. ORIGINAL RSSI AND PDOA DATA ACQUISITION AND PROCESSING

In this section, we simulate the indoor propagation environment of RFID signals [49]–[51] to complete RSSI and PDOA data acquisition and processing, in which the logarithmic path loss model and basic phase-distance model in (2) and (3) are used to obtain the original RSSI and PDOA data, respectively, with RFID reader and tag synchronization not required.

According to the RSSI and PDOA data obtained from different readers, the fingerprint features of RSSI and PDOA for the ith reference tag location can be obtained. The datasets are produced as grid-based structures, in which the RSSI and PDOA datasets of the ith tag can be expressed as $\boldsymbol{s}^i = (s_1^i, s_2^i, s_3^i, \cdots, s_M^i)$ and $\boldsymbol{\phi}^i = (\phi_1^i, \phi_2^i, \phi_3^i, \cdots, \phi_M^i)$, respectively, where M denotes the number of the RFID readers. Since the RFID signal is reflected and diffracted several times, the RSSI and PDOA data can stand for the features of a tag. Thus, the fingerprinting-based RFID localization can be implemented.

In practical applications, the coordinates of the reference tags and the original RSSI and PDOA data at different readers are recorded simultaneously when training samples are collected. After the original RSSI and PDOA data is obtained at N different locations, the RSSI sample set can be expressed as $\boldsymbol{S} = \{(\boldsymbol{s}^1, \boldsymbol{l}^1), (\boldsymbol{s}^2, \boldsymbol{l}^2), \cdots, (\boldsymbol{s}^N, \boldsymbol{l}^N)\}$ and the PDOA sample set can be written as $\boldsymbol{\Phi} = \{(\boldsymbol{\phi}^1, \boldsymbol{l}^1), (\boldsymbol{\phi}^2, \boldsymbol{l}^2), \cdots, (\boldsymbol{\phi}^N, \boldsymbol{l}^N)\}$, where $\boldsymbol{s}^i$ and $\boldsymbol{\phi}^i$ represent the original RSSI and PDOA datasets of the ith tag, respectively, and $\boldsymbol{l}^i$ denotes the position coordinate information of the ith tag.

To facilitate the training of the model and prevent the imbalance in the training procedure, an approximate normalization processing is also required, which is given by

$$\boldsymbol{s}^i = \frac{\boldsymbol{s}^i - \min(\boldsymbol{s})}{\max(\boldsymbol{s}) - \min(\boldsymbol{s})} \quad (4)$$

$$\boldsymbol{\phi}^i = \frac{\boldsymbol{\phi}^i - \min(\boldsymbol{\phi})}{\max(\boldsymbol{\phi}) - \min(\boldsymbol{\phi})} \quad (5)$$

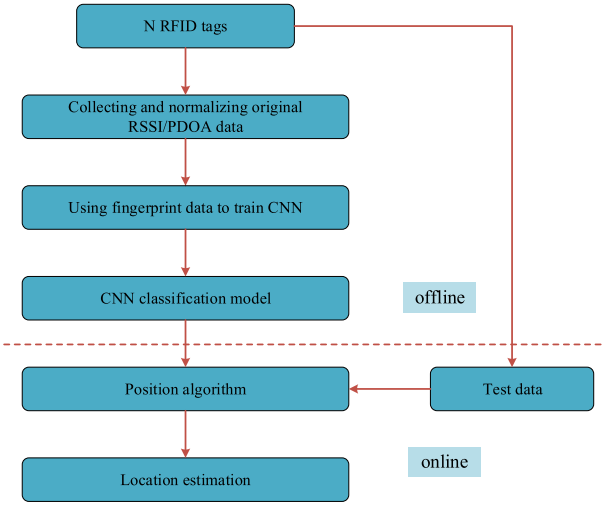

FIGURE 3. RFID localization architecture based on CNN.

It can be seen that the proposed RFID localization approach is to extract fingerprint features of joint RSSI and PDOA datasets via training, so that the characteristics of tags in different positions are more distinctable.

III. CNN-BASED RFID TAG LOCALIZATION VIA JOINT FINGERPRINT FEATURES

A. LOCATION SYSTEM ARCHITECTURE

The RFID localization architecture based on CNN is illustrated in Fig. 3. In the design, the original RSSI and PDOA data of the N reference tags are collected by eight RFID readers, and the original RSSI and PDOA data are normalized to form the training set $\boldsymbol{S}$. Deep learning is performed on the training set information of the N reference tags by using the convolutional neural network. Then the BP algorithm is used to optimize network parameters of CNN by comparing the error between the output and target vectors. In the online test stage, the RSSI and PDOA data of test tags are collected to generate test sets, and the probability distribution matrices are obtained by CNN to achieve localization.

For the CNN-based approach, supervised learning is used to extract the features of fingerprint database and online fingerprint data, respectively. Since the CNN has excellent fitting ability for each group of data, the tag location coordination is determined according to the characteristics of the designed CNN in this paper. Compared with the previous schemes, the CNN-based approach has the following advantages:

1) It has superior two-dimensional data processing and learning ability, which can achieve higher positioning accuracy.
2) The parameters of each layer are shared, so the training time is shorter than that of other neural network approaches such as DNN and DBN.
3) In the collection of fingerprint data sets, reference tags can be reused, which saves the cost of the location system and is helpful for the recycling of resources.

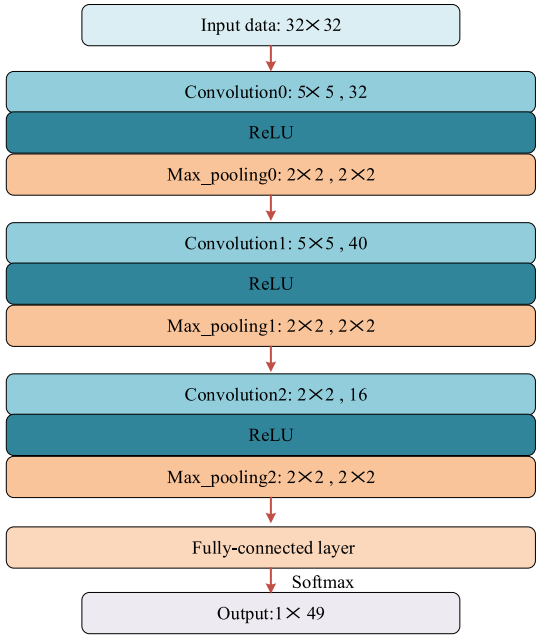

FIGURE 4. The training procedure and parameters of the designed CNN model.

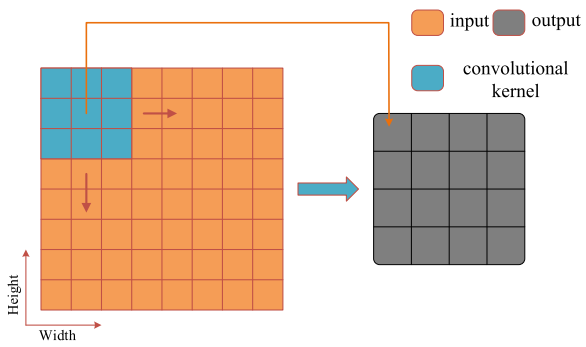

FIGURE 5. Operation of convolution layer.

B. OFFLINE TRAINING

The CNN is an artificial neural network with weight sharing network structure. It is more similar to biological neural network, which is helpful for reducing the number of weights and the complexity of network model. This advantage is more obvious when the network input is a multi-dimensional image. Thus, the image can be directly used as the input of the network, and avoid the process of complicated feature extraction and data reconstruction in the traditional recognition algorithms. As a multi-layer perception specially designed for recognizing two-dimensional shape, the network structure of CNN is highly invariant to translation and scale. Its structure is composed of convolutional layer, pooling layer and fully-connection layer. Fig. 4 shows the training procedure and parameters using the designed CNN model in our approach, and Fig. 5 illustrates the operation of the convolutional layer.

As shown in Fig. 5, the convolutional layer can extract data features from the input feature map and learn the contour of

the map. We define the ith feature map of layer l as h_i^l, which is given by

$$h_i^l = \sigma\Big(\sum_{n\in H_{l-1}} w_{in}^l h_n^{l-1} + b_i^l\Big) \tag{6}$$

where w_{in}^l denotes the convolution kernel, which convolutes with the nth feature map in layer $l-1$ to generate the ith feature map in layer l, the weights are identical for different n feature maps due to local weight sharing. b_i^l is the bias of the ith feature map in layer l. H_{l-1} is the set of output feature maps of layer $l-1$, as the input of layer l. $\sigma(x) = max(0, x)$ is the activation function. ReLU is used as the activation function since it is more efficient in gradient descent and back propagation. In addition, ReLU function can avoid the problem of gradient explosion and gradient disappearance.

Then we employ the output feature maps of convolution layer as the input of pooling layer. The pooling layer can reduce the dimension of features, compress the number of data and parameters, reduce over-fitting, and improve the fault tolerance of the model, also, it is invariant to distortions on the inputs. There are two kinds of pooling functions: max pooling function and mean pooling function. The max pooling function is to take the maximum value of the local region of the feature map, and the mean pooling function is to take the mean value of the local region of the feature map. The max pooling function is used in our approach, which is given by

$$h_{im}^{l+1} = \max_{i\in H^l}\{h_{im}^l\} \tag{7}$$

where H^l is the set of pooling feature map of layer l, and h_{im}^l is the mth pooling region in the ith feature map of layer l. h_{im}^{l+1} is the mth value in the ith feature map of layer l.

We take all the feature images as the input $\boldsymbol{x}$ of the fully-connected layer, then $\boldsymbol{z} = \boldsymbol{w}\boldsymbol{x} + \boldsymbol{b}$ is the output of fully-connected layer, where $\boldsymbol{w}$ and $\boldsymbol{b}$ are the weights and biases of the fully-connected layer, respectively. Assuming that the number of reference tags is N, and $\boldsymbol{z} = [z_1, z_2, \ldots, z_N]$ is a $1 \times N$ row vector, we can obtain the output probability $\boldsymbol{p} = [p_1, p_2, \ldots, p_N]^T$, where

$$p_i = \frac{e^{z_i}}{\sum_{i=1}^{N} e^{z_i}} \tag{8}$$

for $i = 1, \ldots, N$. Then $\boldsymbol{p}$ contains the probability distribution of the test tags at the positions of N reference tags. Moreover, the loss function is used to measure the difference between the true location label and the CNN output $\boldsymbol{p}$. By minimizing the value of loss function with BP algorithm, we can update the weights and biases with stochastic gradient descent method. In the offline training stage, we use the cross-entropy loss function to train the parameters of the neural network, which is written as

$$Los = -\sum_{i=1}^{N} y_i \log p_i \tag{9}$$

where y_i is the true label of the ith location of reference tags, in which we use one-hot code for y_i. The ith value of y_i is 1, and the other $N-1$ values are 0.

The data training procedure for the CNN is shown in Fig. 4. We construct RSSI and PDOA data images with size 32×32. It is convenient for CNN to process images in its convolution and pooling layers. For each input image in the first convolutional and pooling layer, we employ 32 convolutional kernels with size 5×5 to obtain the same number of feature maps with size 28×28, which can extract different characteristics. In order to solve gradient dissipation and accelerate convergence, ReLU function is added between convolution layer and pooling layer. To reduce training data and guarantee the invariance of feature maps, the same number of feature maps with size 14×14 is obtained by pooling with size 2×2. Then, by implementing two more convolutional and pooling layers as in Fig. 4, we obtain the output feature map of the third pooling layer and use it as the input of the full-connection layer. Finally, we obtain a probability distribution vector with size $1\times N$ from the output of full-connection layer using (8), and then combine the label of training data, which can be used to update the training weights such as the convolutional kernels and bias based on the loss function of the BP algorithm.

C. LOCATION ESTIMATION

In the online testing stage, we collect the RSSI/PDOA data of the test tags to generate the test images. The test images are used as the input of CNN to obtain the probability distribution $\boldsymbol{p}$. We totally collect G images for each test tags, and obtain a probability distribution matrix $\boldsymbol{P} = [\boldsymbol{p}^1, \boldsymbol{p}^2, \ldots, \boldsymbol{p}^G]^T$ for each $\boldsymbol{p}^i$. To estimate the tag locations with high-accuracy, we propose a greedy method to select K maximum probabilities and combine the discount factor $\boldsymbol{\delta} = [\delta_1, \delta_2, \ldots, \delta_K]$ to compute a weighted average of these p_j^i, then combine the location of p_j^i corresponding the reference tag as the estimated location of the test tag, which is given by

$$\hat{l} = \frac{1}{G}\sum_{i=1}^{G}\sum_{j=1}^{K} \delta_j l_i^j \frac{p_j^i}{\sum_{m=1}^{K} p_m^i} \tag{10}$$

where l_i^j is the coordinate of the reference tag with respect to p_j^i, and δ_j is the jth discount factor. In the simulation, we found that the reference point with higher probability is more representative, so we set $\boldsymbol{\delta} = [1, 0.2, 0.05, 0.05]$.

IV. ANALYSIS OF EXPERIMENTAL RESULT

A. EXPERIMENTAL ENVIRONMENT AND PARAMETER SETTINGS

In the experiment, the simulation is completed by using PyCharm2018.2 platform and Python3.6 on a computer with CPU 8750H and GPU GTX1050Ti. We use the path-loss model and phase-distances model to simulate the RFID signal propagation between the tag and the reader in the indoor environment, and establish the offline fingerprint database. A square plane with $12m\times12m$ is considered and 8 readers are selected for the positioning environment. As shown

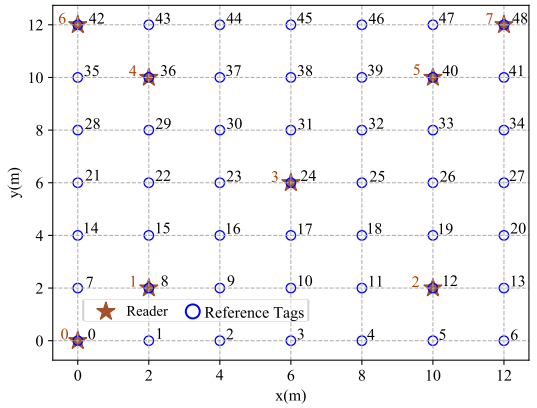

FIGURE 6. Layout of location scene for RFID readers and reference tags.

TABLE 1. Parameters of RFID system.

Parameter	Value
Carrier Frequency f	920 MHz
Transmitter Antenna Gain G_t	8 dBi
receiver Antenna Gain G_r	8 dBi
Transmit Power P_t	30 dBm
The standard variance of Gaussian noise σ_1	$\sqrt{5}$
The standard variance of Gaussian noise σ_2	$\sqrt{10}$
The path loss constant n	2
The number of collecting images G	2
The number of maximum probability points K	4
Room Width and Length	$12m \times 12m$
Number of Readers M	8
Number of reference Tags N	49
Number of test Tags T	50
CNN training iterations	500

in Fig. 6, we select 49 reference tags distributed along uniform distance and label them $\{0, 1, 2, \ldots, 48\}$, and assume that the position coordinates of the reader and reference tags are known. The parameters of the RFID system in the experiment are listed in TABLE 1.

In this paper, we use the mean sum error E as the performance metric of localization algorithms. Assume that the real location of the test tag is (x_i, y_i) and the estimated location is $(\overline{x}, \overline{y})$. The error E for T test tags is calculated as

$$E = \frac{1}{T}\sum_{i=1}^{T}\sqrt{(x_i - \overline{x})^2 + (y_i - \overline{y})^2} \tag{11}$$

In particular, to compare the positioning accuracy of RSSI and PDOA, we design three datasets: RSSI dataset, PDOA dataset, and joint RSSI/PDOA dataset. For the RSSI dataset, we obtain the RSSI values of 8 readers at the ith tag according to (1) by collecting 128 times and normalizing them using (4). Then we use the 128×8 RSSI data to construct one image with size 32×32. For the PDOA dataset, its collection method is the same with RSSI dataset. For the joint RSSI/PDOA dataset, we acquire the RSSI and PDOA values of 8 readers at the ith tag according to (1)(2) and (3) by collecting 64 times and normalizing them using (5). Then we use the 64×16 RSSI and PDOA data to construct one image with size 32×32. Fig. 7 shows the constructed fingerprint images associated with 49 reference tags based on joint RSSI and PDOA data,

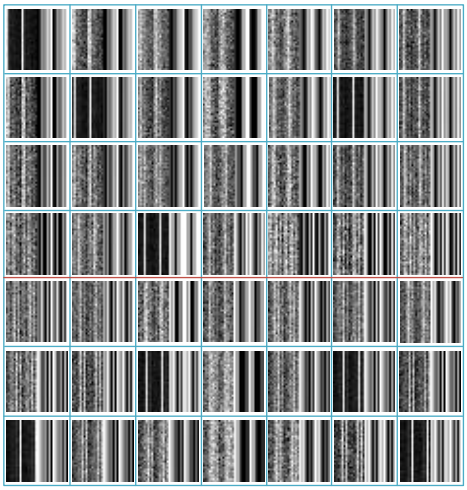

FIGURE 7. The constructed fingerprint images associated with 49 reference tags.

from which it can be observed that each image has its own characteristics. In the experiment, we collect 25 images at each reference tag for the training dataset, and two images for the test dataset.

B. LOCALIZATION PERFORMANCE

Fig. 8 presents the training errors over the iterations of CNN for the three different training datasets. We set the number of training iterations to be 500 to guarantee the successful training, and the training time is about 550s. For the RSSI training dataset, the curves of training error and accuracy begin to converge after 100 iterations, and finally reach about 3×10^{-4} training error and 0.998 training accuracy after 500 iterations. For the PDOA training dataset, the curves of training error and accuracy begin to converge after 80 iterations, and finally reach about 1×10^{-4} training error and 0.999 training accuracy after 500 iterations. For the joint RSSI/PDOA training dataset, the curves of training error and accuracy begin to converge after 40 iterations, and finally reach about 4×10^{-5} training error and 0.999 training accuracy after 500 iterations. From the three different training data we can see that, the method with joint RSSI/PDOA training data has the fastest converge velocities of training error and accuracy, and its curves are more smoothly than the other two training data. The reason is that abundant and distinct fingerprint characteristics are exploited.

To validate the superiority of the proposed CNN-based approach, we compare it with several other fingerprinting location schemes such as LANDMARC [26], WKNN [20] and DNN [40]. LANDMARC belongs to the machine learning methods, in which the location estimation is carried out by selecting the reference tags nearest to the location tags. WKNN calculates the weights corresponding to the K locations and performs a weighted average method as the estimation result. DNN needs a mass of data to offline train as a deep learning-based method, in which multi-hidden layers are constructed and network parameters are optimized by using BP algorithm. We randomly generate 50 test tags, and set

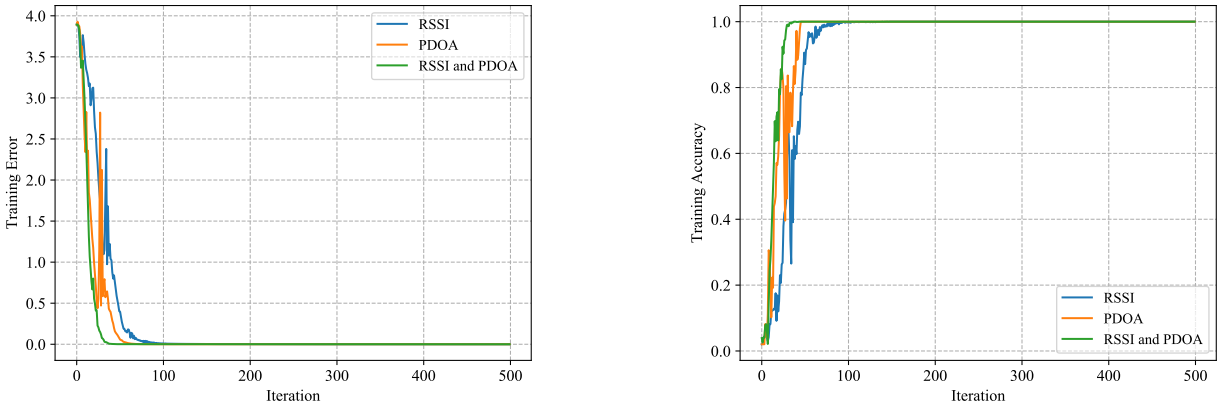

(a) Training errors (b) Training accuracy

FIGURE 8. Training errors and training accuracies over the iterations of CNN for three different training data: RSSI, PDOA, RSSI/PDOA.

TABLE 2. Mean error and execution time (RSSI).

Algorithm	Mean err. (m)	Std. dev. (m)	Mean time (ms)
CNN	1.130	0.537	27.4
DNN	1.224	0.563	17.6
LANDMARC	1.599	1.001	1.3
WKNN	1.626	1.014	1.3

TABLE 3. Mean error and execution time (PDOA).

Algorithm	Mean err. (m)	Std. dev. (m)	Mean time (ms)
CNN	0.681	0.399	27.4
DNN	0.806	0.521	17.8
LANDMARC	1.004	0.628	1.3
WKNN	1.012	0.630	1.3

TABLE 4. Mean error and execution time (Joint RSSI and PDOA).

Algorithm	Mean err. (m)	Std. dev. (m)	Mean time (ms)
CNN	0.667	0.382	26.8
DNN	0.784	0.516	17.8
LANDMARC	1.038	0.660	3.5
WKNN	1.072	0.664	3.4

$\sigma_1^2 = 5$ and $\sigma_2^2 = 10$. The performance of RFID localization approaches using CNN, DNN, LANDMARC and WKNN are compared under three different training and test datasets including RSSI, PDOA, joint RSSI/PDOA, respectively. For a fair comparison, the four approaches use the identical RSSI and PDOA datasets.

TABLE 2-4 illustrates the comparison of mean error and executive time using the CNN, DNN, LANDMARC and WKNN based approaches for different datasets. For the RSSI dataset, we can see from TABLE 2 that the CNN-based approach can achieve a mean location error of $1.130m$ and a standard deviation of $0.537m$ for the 50 test tags. For the PDOA dataset, we find from TABLE 3 that its error is lower than using the RSSI dataset due to the stronger linear relationship between PDOA fingerprint and distance, thus the CNN-based approach can obtain a mean error of $0.681m$ and a standard deviation of $0.399m$ for the 50 test points. For the joint RSSI/PDOA dataset, we observe from TABLE 4 that the error of the CNN-based approach has further reduced due to the abundance of fingerprint data, whose mean error and standard deviation have decreased to $0.667m$ and $0.382m$, respectively. In addition, it can be seen that under different fingerprints, the positioning accuracy of CNN is about $0.15m$ higher on average than that of DNN, and about $0.5m$ higher on average than that of LANDMARC and WKNN. Therefore, the CNN-based approach outperforms the other schemes in indoor localization accuracy, and it performs robustness for different locations with the smallest standard deviation. In addition, to examine the computational complexity, we compare the execution time of the CNN, DNN, LANDMARC and WKNN based approaches. It is shown that the average execution time of the CNN approach is about $27ms$, which is larger than the contrast schemes. Nevertheless, it can satisfy the real-time requirement for most indoor localization applications.

Fig. 9 shows the cumulative distribution function (CDF) versus positioning error for different fingerprint positioning schemes, including CNN, DNN, LANDMARC and WKNN. We consider three different test datasets: RSSI, PDOA and joint RSSI/PDOA.

In Fig. 9(a), the RSSI dataset is used with $\sigma_1^2 = 5$. It can be seen that the CNN-based approach has significantly better performance than the others, in which 75% of the test tags are guaranteed to have an error under $1m$. For DNN, only about 42% of the test tag errors are guaranteed to be within $1m$, and for LANDMARC and WKNN, only about 22% of the test tags have an error within $1m$. In addition, CNN and DNN have approximate 95% of the test tag errors within 2m, while LANDMARC and WKNN have the same test points with mean error under $3m$. Since the neural network-based algorithms such as CNN and DNN can deeply learn data features, their localization effect is more stable and reliable than that of conventional approaches such as LANDMARC and WKNN.

In Fig. 9(b), the PDOA dataset is used with $\sigma_2^2 = 10$. We can see that in the complex indoor propagation environment, the CNN-based approach can achieve a $1m$ distance error for over 80% of the test points, and almost all the tag errors are guaranteed to be within 2 m, which is the most

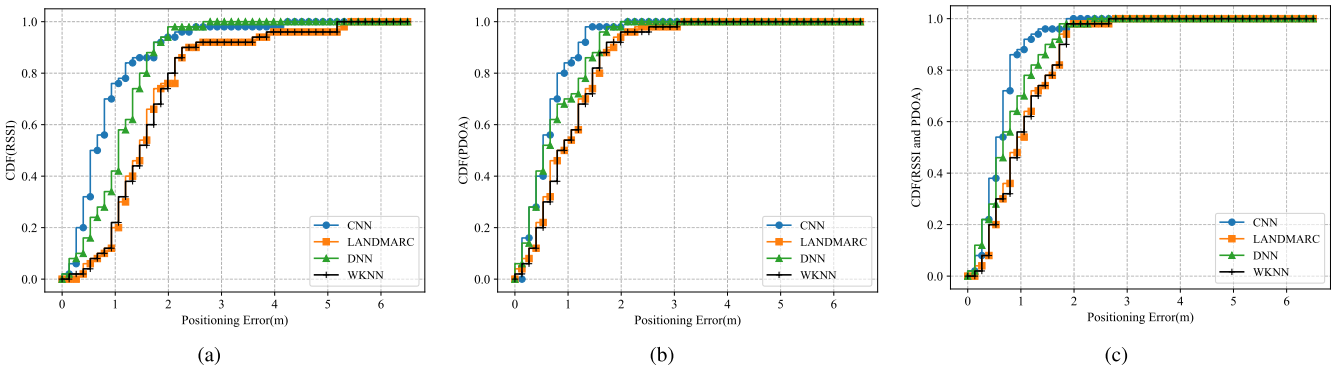

FIGURE 9. Comparison of cumulative distribution function of location error for different approaches under three test datasets. (a) RSSI; (b) PDOA; (c) joint RSSI/PDOA.

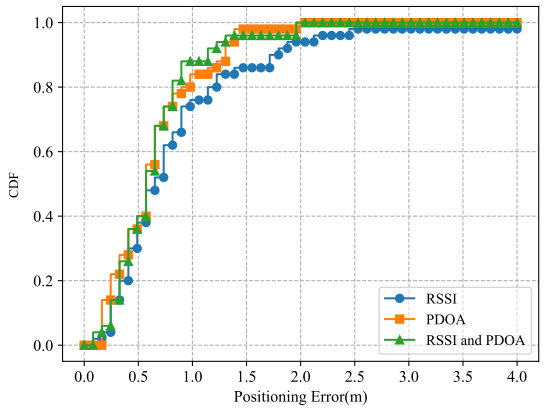

FIGURE 10. Cumulative distribution function of location error for the CNN-based approach under three different test datasets.

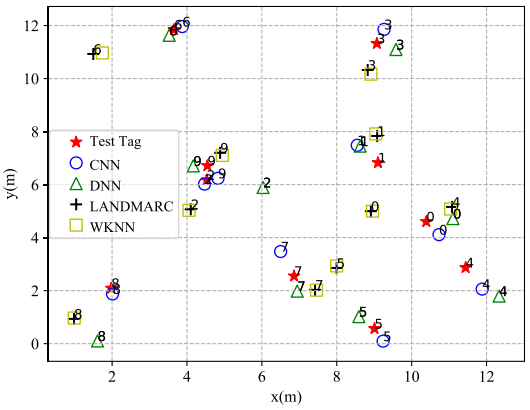

FIGURE 11. Location estimation results of four different approaches.

accurate among the four schemes. For LANDMARC and WKNN, only 50% of the test points have a $1m$ distance error. Since the CNN approach can explore two-dimensional data information in comparison with DNN, it can achieve higher accuracy even with a simple network structure. Also, the phase information is more robust than amplitude since the phase of the signal periodically changes over the propagation distance, especially in cluttered propagation environment. Therefore, the method using the PDOA dataset has better location performance than using the RSSI dataset.

In Fig. 9(c), the joint RSSI/PDOA dataset is used with $\sigma_1^2 = 5$ and $\sigma_2^2 = 10$. We can observe that with more abundant RSSI and PDOA data information, the proposed CNN approach can achieve about 90% of the test points with a distance error under $1m$. However, DNN has the same portion of test points with error under $1.5m$, and LANDMARC and WKNN are with errors under about $1.8m$. At the same time, all the four algorithms can ensure the positioning error within $2m$, which indicates that rich fingerprint information has improved the positioning accuracy.

Fig. 10 shows the CDF of location error of the CNN-based approach under the three different test datasets. It indicates that under the RSSI, PDOA and joint RSSI/PDOA datasets, the CNN-based approach has approximate 90% of the test points with mean location errors under $1.7m$, $1.3m$ and $1m$, respectively. Therefore, the joint RSSI/PDOA dataset can bring the highest accuracy among the three datasets since richer fingerprint information can be provided. Compared with the RSSI dataset, the positioning effect using the PDOA dataset can be greatly improved. The reason is that the phase of the signal periodically changes over the propagation distance, which is linearly related to distance. Thus, the relationship between collected data and tag location is more obvious. In comparison with the RSSI dataset in which the signal amplitude is non-linearly related to distance, the use of the PDOA dataset can achieve better positioning performance.

Fig. 11 intuitively illustrates the location estimation results of the four different approaches. In the area of $12m \times 12m$, we randomly generate 10 test points and collect their RSSI and PDOA data. The number of the 10 test tags is labeled $\{0, 1, \ldots, 9\}$. As seen from Fig. 11, the proposed CNN-based algorithm outperforms all the other schemes (i.e., DNN, LANDMARC, and WKNN) for most points. For the LANDMARC and WKNN methods, the estimated positions of most test points are far from the true values, and their positioning effects are poor. Especially with regard to the eighth tag, we can observe that due to the presence of noise, even if the test tag falls into the reference tag position, they still have large location errors, while CNN has an excellent positioning effect. Moreover, for the neural network based algorithms (i.e., CNN, DNN), the estimated locations of the test points are close to their true values, while the CNN approach has

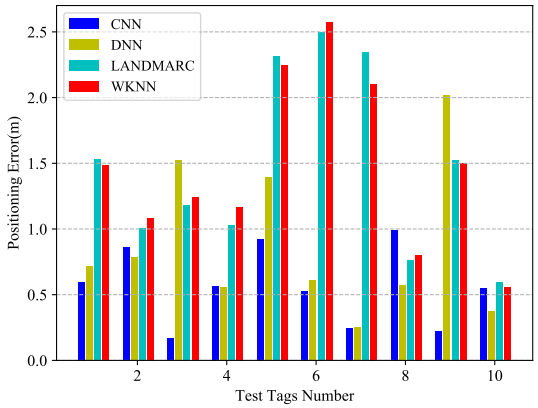

FIGURE 12. Positioning error comparison of four different approaches (10 test points).

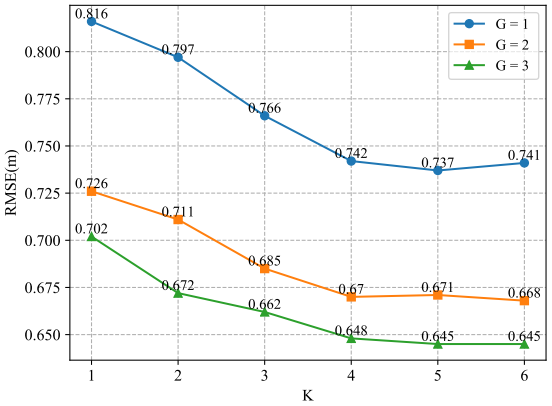

FIGURE 13. Positioning effect under different K and G.

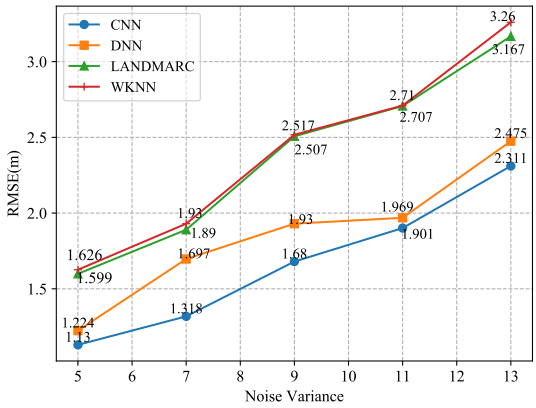

FIGURE 14. RMSE v.s σ_1^2 for different approaches.

smaller positioning error than the DNN approach, and its location effect is outstanding.

Fig. 12 shows the comparison result of the positioning error of the four different algorithms. We use the same 10 test tags as in Fig. 11. It is shown from Fig. 12 that for almost all the test tags, the positioning errors of the CNN and DNN approaches are smaller than those of the LANDMARC and WKNN methods. Specifically, the positioning errors of the 10 test tags using CNN are all below $1m$, though there are three test tags have higher positioning errors than DNN. However, the positioning errors of only 4 points are below $1m$ for the LANDMARC and WKNN approaches. Also, their stability of localization is obviously inferior to that of CNN.

C. IMPACT OF ALGORITHM PARAMETER AND ENVIRONMENT VARIATION

Different parameters K and G in the positioning algorithm will affect the positioning accuracy, thus we explore the impact of K and G. In the experiment, assume that K changes from 1 to 6 and $G = 1, 2, 3$. In addition, noise will affect the relationship between the distance and fingerprint data (i.e., RSSI, PDOA), so we investigate the impact of noise on RSSI and PDOA characteristics via changing the noise variances in the path-loss model and the phase-distance model, respectively. The noise variances σ_1^2 changes from 5 to 13 and σ_2^2 from 10 to 120. We respectively collect the RSSI and PDOA data of 50 test tags under different noise variances, and compare the performance of location estimation of the LANDMARC, WKNN, DNN and CNN algorithms. The root mean square error (RMSE) of 50 test tags is calculated for each algorithm.

Fig. 13 shows the positioning effect under different parameters K and G. We can see that when K gradually increases from 1 to 4, the positioning effect becomes better and better. In the three cases $G = 1, 2, 3$, the positioning errors when $K = 4$ are $0.074m$, $0.056m$, $0.054m$, respectively, which are lower than that when $K = 1$. When K is greater than 4, the positioning accuracy is hardly improved and tends to be stable. Therefore, we usually set $K = 4$, which can improve the positioning accuracy while save the running time. Taking $K = 4$ as an example, the positioning error when G changes from 2 to 1 is reduced by $0.072m$, and that when G changes from 3 to 2 is reduced by $0.022m$. It can be seen that the increase of G can slightly improve the positioning accuracy.

Fig. 14 shows the RMSE versus σ_1^2 for different approaches. The experiment is performed using the RSSI dataset. It can be seen that with the increase of σ_1^2, the location errors of LANDMARC and WKNN increase more rapidly than CNN and DNN. Moreover, when σ_1^2 increases from 5 to 11, the increase of positioning errors for the CNN and DNN approaches become slow. Also, when σ_1^2 increases from 5 to 13, the error of CNN only increases by $1.181m$, while the errors of DNN, WKNN and LANDMARC can increase by $1.233m$, $1.568m$ and $1.634m$, respectively. In the case of the same noise variance σ_1^2, the proposed CNN-based approach performs better than other schemes, which indicates that it has better robustness and is more suitable for complex indoor environment.

Fig. 15 presents the RMSE versus σ_2^2 for different approaches. The experiment is based on the PDOA dataset. We can see that compared with the other three positioning schemes, the proposed CNN-based approach can still achieve excellent positioning results when the noise variance σ_2^2 is large. With the increase of σ_2^2, the location error of the CNN approach increase slower than that of other schemes.

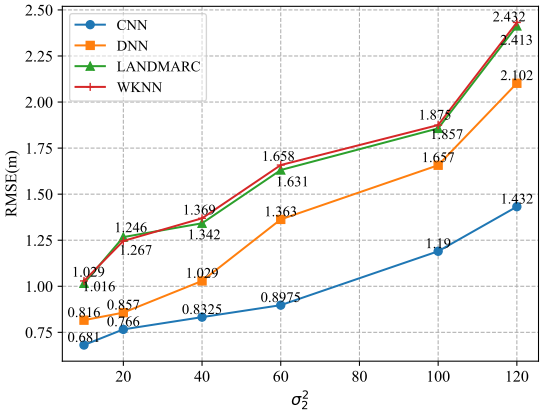

FIGURE 15. RMSE v.s σ_2^2 for different approaches.

Also, when σ_2^2 increases from 10 to 120, the error of CNN only increases by $0.751m$, while the errors of DNN, WKNN and LANDMARC increase by $1.286m$, $1.397m$ and $1.407m$, respectively. Moreover, Fig. 14 and Fig. 15 illustrate that the positioning accuracy using the PDOA dataset has greatly improved in comparison with using the RSSI dataset. The position fingerprint of PDOA is more stable and superior than RSSI when the environment becomes harsh, since PDOA has better data characteristics due to its linear relationship with distance.

V. CONCLUSION

In this paper, a deep CNN-based approach for passive RFID tag localization is proposed by exploiting joint fingerprint features of the RSSI and PDOA. The RSSI and PDOA data are collected and normalized by arranging RFID readers and tags. In the offline phase, the CNN with three convolution layers and pooling layers is used to learn the characteristics of the normalized data deeply, and the network parameters are optimized using the BP algorithm. In the online test phase, the trained CNN model are used to output the probability distribution of the test data, combined with a greedy method to improve the accuracy. The positioning effect of the proposed CNN-based approach is validated by three different types of datasets. It is found that the PDOA dataset performs better than the RSSI dataset, and the joint RSSI/PDOA dataset performs the best in positioning effect. The experiments show that the proposed deep learning-based approach is superior to the traditional fingerprinting-based schemes and more suitable for RFID tag localization in complex indoor environment.

REFERENCES

[1] J. Zhang, Y. Lyu, J. Patton, S. C. G. Periaswamy, and T. Roppel, "BFVP: A probabilistic UHF RFID tag localization algorithm using Bayesian filter and a variable power RFID model," *IEEE Trans. Ind. Electron.*, vol. 65, no. 10, pp. 8250–8259, Oct. 2018.

[2] W. Zhu, J. Cao, Y. Xu, L. Yang, and J. Kong, "Fault-tolerant RFID reader localization based on passive RFID tags," *IEEE Trans. Parallel Distrib. Syst.*, vol. 25, no. 8, pp. 2065–2076, Aug. 2014.

[3] B. S. Ciftler, A. Kadri, and I. Guvenc, "IoT localization for bistatic passive UHF RFID systems with 3-D radiation pattern," *IEEE Internet Things J.*, vol. 4, no. 4, pp. 905–916, Aug. 2017.

[4] P. Yang and W. Wu, "Efficient particle filter localization algorithm in dense passive RFID tag environment," *IEEE Trans. Ind. Electron.*, vol. 61, no. 10, pp. 5641–5651, Oct. 2014.

[5] J.-M. Akre, X. Zhang, S. Baey, B. Kervella, A. Fladenmuller, M. A. Zancanaro, and M. Fonseca, "Accurate 2-D localization of RFID tags using antenna transmission power control," in *Proc. IFIP Wireless Days (WD)*, Rio de Janeiro, Brazil, Nov. 2014, pp. 1–6.

[6] J. Lai, C. Luo, J. Wu, J. Li, J. Wang, J. Chen, G. Feng, and H. Song, "TagSort: Accurate relative localization exploring RFID phase spectrum matching for Internet of Things," *IEEE Internet Things J.*, vol. 7, no. 1, pp. 389–399, Jan. 2020.

[7] A. Buffi, P. Nepa, and F. Lombardini, "A phase-based technique for localization of UHF-RFID tags moving on a conveyor belt: Performance analysis and test-case measurements," *IEEE Sensors J.*, vol. 15, no. 1, pp. 387–396, Jan. 2015.

[8] G. Shi, Y. He, B. Yin, L. Zuo, P. She, W. Zeng, and F. Ali, "Analysis of mutual couple effect of UHF RFID antenna for the Internet of Things environment," *IEEE Access*, vol. 7, pp. 81451–81465, 2019.

[9] Y. Zuo, "Survivable RFID systems: Issues, challenges, and techniques," *IEEE Trans. Syst., Man, Cybern. C, Appl. Rev.*, vol. 40, no. 4, pp. 406–418, Jul. 2010.

[10] X. Jia, Q. Feng, T. Fan, and Q. Lei, "RFID technology and its applications in Internet of Things (IoT)," in *Proc. 2nd Int. Conf. Consum. Electron., Commun. Netw. (CECNet)*, Yichang, China, Apr. 2012, pp. 1282–1285.

[11] S. F. Wamba and E. W. T. Ngai, "Importance of the relative advantage of RFID as enabler of asset management in the healthcare: Results from a delphi study," in *Proc. 45th Hawaii Int. Conf. Syst. Sci.*, Jan. 2012, pp. 2879–2889.

[12] T. D. Räty, "Survey on contemporary remote surveillance systems for public safety," *IEEE Trans. Syst., Man, Cybern. C, Appl. Rev.*, vol. 40, no. 5, pp. 493–515, Sep. 2010.

[13] E. Welbourne, L. Battle, G. Cole, K. Gould, K. Rector, S. Raymer, M. Balazinska, and G. Borriello, "Building the Internet of Things using RFID: The RFID ecosystem experience," *IEEE Internet Comput.*, vol. 13, no. 3, pp. 48–55, May 2009.

[14] G. Kortuem, F. Kawsar, V. Sundramoorthy, and D. Fitton, "Smart objects as building blocks for the Internet of Things," *IEEE Internet Comput.*, vol. 14, no. 1, pp. 44–51, Jan. 2010.

[15] I. Guvenc, S. Gezici, and Z. Sahinoglu, "Fundamental limits and improved algorithms for linear least-squares wireless position estimation," *Wireless Commun. Mobile Comput.*, vol. 12, no. 12, pp. 1037–1052, Aug. 2012.

[16] Y. Gu, A. Lo, and I. Niemegeers, "A survey of indoor positioning systems for wireless personal networks," *IEEE Commun. Surveys Tuts.*, vol. 11, no. 1, pp. 13–32, 1st Quart., 2009.

[17] H. Liu, H. Darabi, P. Banerjee, and J. Liu, "Survey of wireless indoor positioning techniques and systems," *IEEE Trans. Syst., Man, Cybern. C, Appl. Rev.*, vol. 37, no. 6, pp. 1067–1080, Nov. 2007.

[18] X. Fu, A. Pedross-Engel, D. Arnitz, and M. S. Reynolds, "Simultaneous sensor localization via synthetic aperture radar (SAR) imaging," in *Proc. IEEE Sensors*, Orlando, FL, USA, Oct. 2016, pp. 1–3.

[19] M. Gareis, P. Fenske, C. Carlowitz, and M. Vossiek, "Particle filter-based SAR approach and trajectory optimization for real-time 3D UHF-RFID tag localization," in *Proc. IEEE Int. Conf. RFID (RFID)*, Orlando, FL, USA, Sep. 2020, pp. 1–8.

[20] Z. Belhadi and L. Fergani, "Fingerprinting methods for RFID tag indoor localization," in *Proc. Int. Conf. Multimedia Comput. Syst. (ICMCS)*, Marrakech, Morocco, Apr. 2014, pp. 717–722.

[21] A. A. Nazari Shirehjini and S. Shirmohammadi, "Improving accuracy and robustness in HF-RFID-Based indoor positioning with Kalman filtering and tukey smoothing," *IEEE Trans. Instrum. Meas.*, vol. 69, no. 11, pp. 9190–9202, Nov. 2020.

[22] A. G. Dimitriou, "Design, analysis, and performance evaluation of a UHF RFID forward-link repeater," *IEEE J. Radio Freq. Identificat.*, vol. 4, no. 2, pp. 73–82, Jun. 2020.

[23] W. Xu, Y. Shao-Wei, and H. Zi-Shu, "Two kinds of joint location algorithms of TDOA and TOA for TDMA system targets," in *Proc. Int. Conf. App. Comput. and Intell. Anal. Process. (ICACIA)*, Chengdu, China, 2010, pp. 84–88.

[24] Y. Wang and K. C. Ho, "An asymptotically efficient estimator in closed-form for 3-D AOA localization using a sensor network," *IEEE Trans. Wireless Commun.*, vol. 14, no. 12, pp. 6524–6535, Dec. 2015.

[25] M. Hasani, E.-S. Lohan, L. Sydanheimo, and L. Ukkonen, "Path-loss model of embroidered passive RFID tag on human body for indoor positioning applications," in *Proc. IEEE RFID Technol. Appl. Conf. (RFID-TA)*, Tampere, Finland, Sep. 2014, pp. 170–174.

[26] Y. Xie, Z. Wang, and S. Zheng, "On RFID positioning base on LANDMARC and improved algorithm," in *Proc. Chin. Control Conf.*, Beijing, China, 2010, pp. 4831–4836.

[27] K. Chawla, C. McFarland, G. Robins, and C. Shope, "Real-time RFID localization using RSS," in *Proc. Int. Conf. Localization GNSS (ICL-GNSS)*, Turin, Italy, Jun. 2013, pp. 1–6.

[28] Y. Wen, X. Tian, X. Wang, and S. Lu, "Fundamental limits of RSS fingerprinting based indoor localization," in *Proc. IEEE Conf. Comput. Commun. (INFOCOM)*, Hong Kong, Apr. 2015, pp. 2479–2487.

[29] H. Yigit, "A weighting approach for KNN classifier," in *Proc. Int. Conf. Electron., Comput. Comput. (ICECCO)*, Ankara, Turkey, Nov. 2013, pp. 228–231.

[30] H. Wu, B. Tao, Z. Gong, Z. Yin, and H. Ding, "A fast UHF RFID localization method using unwrapped phase-position model," *IEEE Trans. Auto. Sci. Engin.*, vol. 16, no. 4, pp. 1698–1707, Oct. 2019.

[31] Z. Zhang, Z. Lu, V. Saakian, X. Qin, Q. Chen, and L.-R. Zheng, "Item-level indoor localization with passive UHF RFID based on tag interaction analysis," *IEEE Trans. Ind. Electron.*, vol. 61, no. 4, pp. 2122–2135, Apr. 2014.

[32] S. Siachalou, S. Megalou, A. Tzitzis, E. Tsardoulias, A. Bletsas, J. Sahalos, T. Yioultsis, and A. G. Dimitriou, "Robotic inventorying and localization of RFID tags, exploiting phase-fingerprinting," in *Proc. IEEE Int. Conf. RFID Technol. Appl. (RFID-TA)*, Pisa, Italy, Sep. 2019, pp. 362–367.

[33] J. Wang, Y. Ma, Y. Zhao, and K. Liu, "A multipath mitigation localization algorithm based on MDS for passive UHF RFID," *IEEE Commun. Lett.*, vol. 19, no. 9, pp. 1652–1655, Sep. 2015.

[34] M. Wegener, D. Fros, M. Rosler, C. Drechsler, C. Patz, and U. Heinkel, "Relative localisation of passive UHF-tags by phase tracking," in *Proc. 13th Int. Multi-Conf. Syst., Signals Devices (SSD)*, Leipzig, Germany, Mar. 2016, pp. 503–506.

[35] W. Li, X. Wang, and B. Moran, "A lattice method for resolving range ambiguity in dual-frequency RFID tag localisation," in *Proc. IEEE Int. Conf. Acoust., Speech Signal Process. (ICASSP)*, New Orleans, LA, USA, Mar. 2017, pp. 3156–3160.

[36] K. Thangarajah, R. Rashizadeh, S. Erfani, and M. Ahmadi, "A hybrid algorithm for range estimation in RFID systems," in *Proc. 19th IEEE Int. Conf. Electron., Circuits, Syst. (ICECS)*, Seville, Spain, Dec. 2012, pp. 921–924.

[37] E. DiGiampaolo and F. Martinelli, "Mobile robot localization using the phase of passive UHF RFID signals," *IEEE Trans. Ind. Electron.*, vol. 61, no. 1, pp. 365–376, Jan. 2014.

[38] H. Ma and K. Wang, "Fusion of RSS and phase shift using the Kalman filter for RFID tracking," *IEEE Sensors J.*, vol. 17, no. 11, pp. 3551–3558, Jun. 2017.

[39] O. Sharma, "Deep challenges associated with deep learning," in *Proc. Int. Conf. Mach. Learn., Big Data, Cloud Parallel Comput. (COMITCon)*, Faridabad, India, Feb. 2019, pp. 72–75.

[40] W. Zhang, R. Sengupta, J. Fodero, and X. Li, "DeepPositioning: Intelligent fusion of pervasive magnetic field and WiFi fingerprinting for smartphone indoor localization via deep learning," in *Proc. 16th IEEE Int. Conf. Mach. Learn. Appl. (ICMLA)*, Cancun, Mexico, Dec. 2017, pp. 7–13.

[41] C. Zhang, Y. He, S. Jiang, T. Wang, L. Yuan, and B. Li, "Transformer fault diagnosis method based on self-powered RFID sensor tag, DBN, and MKSVM," *IEEE Sensors J.*, vol. 19, no. 18, pp. 8202–8214, Sep. 2019.

[42] X. Wang, X. Wang, and S. Mao, "CiFi: Deep convolutional neural networks for indoor localization with 5GHz Wi-Fi," in *Proc. IEEE ICC*, Paris, French, May 2017, pp. 1–6.

[43] X. Wang, L. Gao, S. Mao, and S. Pandey, "DeepFi: Deep learning for indoor fingerprinting using channel state information," in *Proc. IEEE Wireless Commun. Netw. Conf. (WCNC)*, New Orleans, LA, USA, Mar. 2015, pp. 1666–1671.

[44] X. Wang, L. Gao, and S. Mao, "CSI phase fingerprinting for indoor localization with a deep learning approach," *IEEE Internet Things J.*, vol. 3, no. 6, pp. 1113–1123, Dec. 2016.

[45] H. Jiang, C. Peng, and J. Sun, "Deep belief network for fingerprinting-based RFID indoor localization," in *Proc. IEEE Int. Conf. Commun. (ICC)*, Shanghai, China, May 2019, pp. 1–5.

[46] A. Bekkali, S. Zou, A. Kadri, M. Crisp, and R. Penty, "Performance analysis of passive UHF RFID systems under cascaded fading channels and interference effects," *IEEE Trans. Wireless Commun.*, vol. 14, no. 3, pp. 1421–1433, Mar. 2015.

[47] G. Li, C. Li, J. Wu, and Y. Yin, "RFID location algorithm based on target search and repeat calibration," *Procedia Comput. Sci.*, vol. 147, pp. 453–457, Dec. 2019.

[48] Z. Li, G. He, M. Li, L. Ma, Q. Chen, J. Huang, J. Cao, S. Feng, H. Gao, and S. Wang, "RBF neural network based RFID indoor localization method using artificial immune system," in *Proc. Chin. Control Decis. Conf. (CCDC)*, Shenyang, China, Jun. 2018, pp. 2837–2842.

[49] E. Leitinger, P. Meissner, M. Frohle, and K. Witrisal, "Performance bounds for multipath-assisted indoor localization on backscatter channels," in *Proc. IEEE Radar Conf.*, Cincinnati, OH, USA, May 2014, pp. 70–75.

[50] Z. Yang, Z. Zhou, and Y. Liu, "From RSSI to CSI: Indoor localization via channel response," *ACM Comput. Surv.*, vol. 46, no. 2, pp. 25–32, Nov. 2013.

[51] D. Liang, Z. Zhang, and M. Peng, "Access point reselection and adaptive cluster splitting-based indoor localization in wireless local area networks," *IEEE Internet Things J.*, vol. 2, no. 6, pp. 573–585, Dec. 2015.

CHAO PENG received the B.S. degree in communication engineering from the College of Communication Engineering, Jilin University, Changchun, China, in 2018, where he is currently pursuing the M.S. degree in information and communication engineering. His research interests include deep learning with applications to indoor localization and radio-frequency identification (RFID) technology.

HONG JIANG (Member, IEEE) received the B.S. degree in radio technology from Tianjin University, Tianjin, China, in 1989, the M.S. degree in communication and electronic systems from the Jilin University of Technology, Changchun, China, in 1996, and the Ph.D. degree in communication and information systems from Jilin University, Changchun, in 2005. From 2010 to 2011, she was a Visiting Scholar with the Department of Electrical and Computer Engineering, McMaster University, Hamilton, ON, Canada. She is currently a Professor with the College of Communication Engineering, Jilin University. Her research interests include array signal processing, target detection and parameter estimation, and signal processing for wireless communication and localization. She is a Senior Member of the Chinese Institute of Electronics.

LIANGDONG QU received the B.S. degree in computer science and technology, the M.S. degree in software engineering, and the Ph.D. degree in computer application technology from Jilin University, Changchun, China, in 2004, 2006, and 2010, respectively. He is currently a Lecturer with the College of Communication Engineering, Jilin University. His research interests include computer networks, artificial intelligence, communication protocol, and embedded systems.